Available online at www.sciencedirect.com
SCIENCE DIRECT®
International Journal of Heat and Mass Transfer 47 (2004) 1217–1226
International Journal of HEAT and MASS TRANSFER
www.elsevier.com/locate/ijhmt

Exploring super-critical properties of secondary flows of natural convection in inclined channels

Hongxing Yang [a,*], Zuojin Zhu [b]

[a] Department of Building Services Engineering, The Hong Kong Polytechnic University, Kowloon, Hong Kong
[b] Department of Thermal Science and Energy Engineering, University of Science and Technology of China, Hefei, Anhui 230026, PR China

Received 2 May 2003; received in revised form 12 September 2003

Abstract

The super-critical secondary flow properties of natural convection in an inclined channel (NCIC) have been explored numerically by virtue of Boussinesq type Navier–Stokes equations. The primary flow in the inclined channel heated from below was assumed as fully developed so that the secondary flow in the cross-section can be studied as a Bénard type problem without regarding the primary speed profiles but allowing the buoyancy force depending on the channel inclination. The ratios of channel spacing to width for the inclined channel have been considered to recognize the sensitivity to the secondary flow patterns from the ratio, with the Rayleigh number changing from 10^4 to 10^6. For moderate Rayleigh numbers ranging from 10^4 to 10^5, it was revealed that the numerically evaluated spatial wavelength of the secondary flow appears a relatively good consistence with measured data, and the pattern of the secondary flow is sensitive to the inclination angle.

1. Introduction

Natural convection has become an ad hoc heat transfer subject in recent two decades, as more and more applications in solar energy, building services engineering and other industrial processes have been found. Elenbaas [1] had considered the natural convection in inclined channels earlier, while Bodoia and Osterle [2] studied the development of natural convection in 1962. A number of important investigations were carried out when solar energy technology was highlighted during 1970s and 1980s. Among these, are the contributions from Aung et al. [3–5], Sparrow et al. [6], and Wirtz and Liu [7]. Not only have these works make sure of the research depth of the subject, but has improved the understanding of its phenomenon.

Actually, to meet the technological demands in applications, the study of natural convection has been intensified. For example, Zanchini [8] and Barletta [9,10] have studied the mixed and natural convection in parallel walled channels by using the perturbation series method. They found the fields of velocity and temperature, and the Nusselt numbers associated with the flow characteristic parameter. Barletta and Zanchini [11] have further studied the time periodic laminar mixed convection in an inclined channel. They derived the oscillations of local velocity, pressure and heat flux, and explored the impacts from the Prandtl number and the angular frequency of the hot wall temperature on these oscillations. This work is of great significance, since for some super-critical cases the secondary flow for the natural convection in the inclined channel can lead to the overall Nusselt number oscillates with heating time.

In addition, there were a number of studies of natural convection associated with particular boundary conditions [12–19]; the transition to unsteady natural convection [20–23], the onset of unsteadiness to chaos [23], and 3D simulation for natural convection in rectangular enclosures [24–27]. This indicates that the study of

* Corresponding author. Tel.: +852-27665863; fax: +852-27657198.
E-mail addresses: behxyang@polyu.edu.hk (H. Yang), zuojin@ustc.edu.cn (Z. Zhu).

0017-9310/$ - see front matter © 2003 Elsevier Ltd. All rights reserved.
doi:10.1016/j.ijheatmasstransfer.2003.09.008

Nomenclature

g	gravitational acceleration, m/s^2
$\mathbf{n}$	unit vector normal to the boundary surface
p	Pressure, Pa
Pr	Prandtl number
Ra	$=g\beta_T(T_{w1}-T_{w2})S^3/\nu\kappa$, Rayleigh number
Nu_{av}	$=-\frac{S}{W}\int_0^{W/S}\left.\frac{\partial\Theta}{\partial y}\right\|_{y=0}\mathrm{d}x$, overall Nusselt number
S	spacing between the parallel walls
T	temperature, K
$\mathbf{u}$	velocity vector
$\mathbf{u}^*$	variable in accurate projection defined, m/s
u_0	reference velocity, m/s
u	velocity component in x-direction, m/s
v	velocity component in y-direction, m/s
W	width of the inclined parallel walled channel
x, y	coordinates, m
t	Time

Greek symbols

β_T	Coefficient of thermal expansion
χ	Pressure potential
Δt	nondimensional time interval
ΔT	$T_{w1}-T_{w2}$, temperature difference, K
ψ	stream function
ρ	Density, kg/m^3
$\boldsymbol{\tau}$	Tangent unit vector on boundary $\partial\Omega$
∇^2	Laplacian operator

Superscripts

n	time level
w	Wall
T	Thermal

natural convection has advanced extensively and at a higher professional level. For natural convection in inclined channels (NCIC), the earlier experiments in water was carried out by Azevedo and Sparrow [28], corresponding to the theoretical work of Lavine [29]. Azevedo and Sparrow used water with Prandtl number close to 5.0 to conduct their experiments, and found that the secondary flow in the cross-section appears in cellular patterns, whose structures are closely related to the Rayleigh number, the spatial wavelength of the secondary flow, or say cell size of the flow pattern. While Lavine has found that for the case of uniform heat flux, for any value of Rayleigh number corresponding to an adverse temperature gradient, the convection flow is unstable, and without any dependence on the base velocity and temperature distribution and inclination.

We have previously studied the thermal-induced flow instability in a horizontal parallel plate channel by using a fractional algorithm in numerical experiments [30]. Further, we have used the accurate projection method [31] to address the characteristics of natural convection in a tall cavity [33] as well as the laminar natural convection in an inclined parallel walled channel [34]. Now, in order to reveal the properties of super-critical secondary flow of natural convection in an inclined channel, we investigated the natural convection problem by using the Boussinesq type Navier–Stokes model with the projection method [33].

Fig. 1 shows the schematic of the problem, in which part (a) gives the inclined channel whose side walls are insulated, while part (b) shows the cross-section of the secondary flow occurs due to bottom heating. The secondary flow is numerically simulated by assuming that the main flow in the channel direction is fully developed. For the super-critical natural convection, the Rayleigh

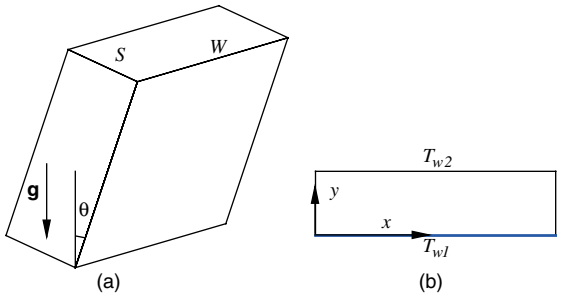

Fig. 1. (a) Schematic diagram of the inclined rectangular channel and (b) secondary flow domain.

number is larger than the critical value and nonlinear effect becomes significant. Because the inclination has affected the buoyancy force component subjecting on the fluid, and the side wall has influence on the number of cells in the cross-section. So far, these features have not been studied in detail. It is necessary to carry out a detailed numerical investigation for the recognization of the secondary flow for NCIC.

2. Governing equations

There are many studies for the natural convection in parallel walled channel. However, as mentioned before, there were less works focused on the corresponding secondary flows, which associated with the inclination and side effects. For convenience, we assume that the fluid is Newtonian type, and the wall temperature difference is small enough, so that the Boussinesq type Navier–Stokes model is still suitable for simulating the

super-critical secondary flows of NCIC. The problem considered has the schematic given in Fig. 1. As theoretically revealed [35], if the inclination angle equals 90°, the critical Rayleigh number of flow in the channel cross-section is 1708. However, when the inclination is small, e.g. less than 45°, the effects of inclination and the influence from the sides are still unsolved issues.

It is assumed that the main stream in the inclined channel is fully developed. The spacing and the width of the channel are respectively labeled by S and W, with the inclination denoted by θ. To describe the secondary flow of fluid having kinematic viscosity v and thermal diffusivity κ, we assume that the side walls are thermally insulated, and the flow is driven by wall temperature difference $T_{w1} - T_{w2}$, with the subscripts "w1" and "w2" indicating the bottom and top walls. The projection of the gravitational acceleration in the cross-section is $g\sin\theta$. Hence, the buoyancy force for driving the secondary flow has decreased by a factor $\sin\theta$, which vanishes as θ is zero, corresponding to the vertical case.

To normalize the governing equations, we use the coordinates given in Fig. 1(b). Following the way of Wakitani [38], we select S and $u_0 = \sqrt{g\beta_T S\Delta T}$ as the units of length and velocity respectively, with time measured by $t_0 = S/u_0 = \sqrt{Pr/Ra}S^2/v$. Hence, if we choose ρu_0^2 as the measure of pressure, and define $\Theta = (T - T_{w2})/\Delta T$, the dimensionless governing equations have the Boussinesq type Navier–Stokes form:

$$\frac{\partial\Theta}{\partial t} + \frac{\partial(u\Theta)}{\partial x} + \frac{\partial(v\Theta)}{\partial y} = \frac{1}{\sqrt{Ra\,Pr}}\nabla^2\Theta \tag{1}$$

$$\frac{\partial u}{\partial x} + \frac{\partial v}{\partial y} = 0 \tag{2}$$

$$\frac{\partial u}{\partial t} + \frac{\partial(uu)}{\partial x} + \frac{\partial(uv)}{\partial y} = -\frac{\partial p}{\partial x} + \sqrt{\frac{Pr}{Ra}}\nabla^2 u \tag{3}$$

$$\frac{\partial v}{\partial t} + \frac{\partial(uv)}{\partial x} + \frac{\partial(vv)}{\partial y} = -\frac{\partial p}{\partial y} + \Theta\sin\theta + \sqrt{\frac{Pr}{Ra}}\nabla^2 v \tag{4}$$

where the inclination is denoted as θ. They can be rewritten as vector forms:

$$\Theta_t + (\mathbf{u}\cdot\nabla)\Theta = \sqrt{1/(PrRa)}\nabla^2\Theta \tag{5}$$

and

$$\nabla\cdot\mathbf{u} = 0 \tag{6}$$

$$\mathbf{u}_t + (\mathbf{u}\cdot\nabla)\mathbf{u} = -\nabla p + \Theta\lambda + \sqrt{Pa/Ra}\nabla^2\mathbf{u} \tag{7}$$

where $\lambda(=(0,\sin\theta))$ is the unit vector in the vertical direction, and Pr is the Prandtl number accompanied by the Rayleigh number denoted as $Ra = g\beta_T(T_{w1} - T_{w2})S^3/v\kappa$.

The solutions of the governing Eqs. (5)–(7) should be sought under appropriate conditions which are compatible with the problem considered. As aforementioned, the boundary conditions on the two vertical walls can be written as:

$$u = 0, \quad v = 0, \quad \Theta = 0 \quad \text{for } y = 1 \tag{8}$$

and

$$u = 0, \quad v = 0, \quad \Theta = 1 \quad \text{for } y = 0 \tag{9}$$

For the horizontal side walls, we have

$$u = 0, \quad v = 0, \quad \partial\Theta/\partial x = 0 \quad \text{for } x = 0 \text{ or } W/S \tag{10}$$

On the other hand, the initial conditions are simply assigned as

$$u = 0, \quad v = 0, \quad \Theta = 0 \quad \text{for } t = 0,\ x, y \in \Omega \tag{11}$$

3. Numerical method

As is well known, the governing equations are available for laminar convections. There are many numerical methods which have been confirmed to be successful in performing physically true solution. Le Quéré and Roquefort [36] have developed a Chebyshev polynomial algorithm, which has been used to analyse the bifurcation of double-diffusive convection with opposing horizontal thermal and solutal gradients [37] and investigate the fluid flow behaviors from onset of steadiness to chaos in a differentially heated square cavity [23]. Wakitani [24] insisted on using the numerical algorithm of Kawamura and Kawahara [39]. There is commonly appreciated finite volume method as described by Patankar [40], and Papanicolaou and Jaluria [41], and finite element method as those appreciated by Khanafer et al. [14].

It is noted that Brown et al. [31] has reported the accurate projection method for Navier–Stokes equations, and confirmed the availability of this method. We have used this method by combining the approximate factorization [32] for the solution of pressure potential field to investigate the natural convection of air in a tall cavity [33]. It was found by rigorously comparing with published data that the projection method is useful in searching the solutions of Boussinesq type Navier–Stokes Equations. A brief description of the procedures of the projection method is as follows:

(1) Introduce a relation between the intermediate velocity vector and the pressure potential first, and then represent the real velocity vector by virtue of a projection operator;
(2) Evaluate the nonlinear convective terms in the governing equation with explicit discretization, and then evaluate the increments of the normalized temperature and velocity components with Crank–Nicolson scheme;

(3) According to these increments, the intermediate velocity vector can be evaluated, and then the Poissonian equation for pressure potential can be solved with approximate factorization method;
(4) Update the velocity vector in terms of the new gradient of the pressure potential;
(5) Return to step 2 if numerical iterations need to continue; Otherwise stop and output the required data.

The intermediate velocity vector is given by

$$\mathbf{u}^* = \mathbf{u} + \nabla\chi \tag{12}$$

where χ is the pressure potential. The projection is written as:

$$\mathbf{u} = \mathbf{P}(\mathbf{u}^*) \tag{13}$$

Thus, the pressure expression can be obtained:

$$p = \left(\frac{\partial}{\partial t} - \frac{1}{2}\sqrt{Pr/Ra}\nabla^2\right)\chi \tag{14}$$

After discretizing the governing equations, we obtain

$$\frac{\Theta^{n+1} - \Theta^n}{\Delta t} = -[(\mathbf{u}\cdot\nabla\Theta)]^{n+\frac{1}{2}} + \frac{1}{2}\sqrt{1/(PrRa)}\nabla^2(\Theta^{n+1} + \Theta^n) \tag{15}$$

$$\frac{\mathbf{u}^{*n+1} - \mathbf{u}^n}{\Delta t} = -[(\mathbf{u}\cdot\nabla\mathbf{u})]^{n+\frac{1}{2}} + [\Theta]^{n+\frac{1}{2}} + \frac{1}{2}\sqrt{Pr/Ra}\nabla^2(\mathbf{u}^{*n+1} + \mathbf{u}^n) \tag{16}$$

$$\mathbf{u}^{n+1} = \mathbf{u}^{*n+1} - \nabla\chi^{n+1} \tag{17}$$

and

$$p^{n+1} = \frac{\chi^{n+1} - \chi^n}{\Delta t} - \frac{1}{2}\sqrt{Pr/Ra}\nabla^2(\chi^{n+1} + \chi^n) \tag{18}$$

where χ satisfies the Poisson's equation

$$\nabla^2\chi = \nabla\cdot\mathbf{u}^* \tag{19}$$

whose boundary conditions are given by

$$\mathbf{n}\cdot\mathbf{u}^* = \mathbf{n}\cdot\mathbf{u}_b, \quad \tau\cdot\mathbf{u}^* = \tau\cdot(\nabla\chi + \mathbf{u}_b) \quad \text{for } x, y \in \partial\Omega \tag{20}$$

Thus

$$\mathbf{n}\cdot\nabla\chi = 0 \quad \text{for } x, y \in \partial\Omega \tag{21}$$

where Ω is the secondary flow domain with its boundary expressed as $\partial\Omega$. As soon as the pressure potential is evaluated, we can update the velocity by

$$\mathbf{u}^{n+1} = \mathbf{u}^{*n+1} - \Delta t\nabla\chi^{n+1} \tag{22}$$

The projection method was named as PmIII, which has second order accuracy for pressure even at grids near the boundaries.

4. Numerical analyses and discussion

4.1. Parameters used in the numerical experiments

Numerical experiments were carried out by using the nearly uniform staggered grid system with grid number 241×49 for the normalized domain $x \in (0, W/S)$, $y \in (0, 1)$ of secondary flow of NCIC. The mesh size close to a wall is assigned as half of that in the core portion of the domain. For any case, the temporal interval was set as 5×10^{-3}. The criteria for the iteration of pressure potential with approximate factorization is 10^{-4} defined by the relative error, as given in Ref. [33], where the issue of grid independence of the numerical method is reported in detail. It shows that using the grid of number 241×49 is quite possible to achieve grid-independent numerical results. The Prandtl number of fluid is set as 5.0, which is the same as that of the fluid in experiments of Azevedo and Sparrow [28].

4.2. Super-critical secondary flow properties

The secondary flows of NCIC, for the super-critical Rayleigh number $Ra = 10^4$, the inclination $\theta = 45$ °C, and the spacing to width ratio 0.1, are constituted by totally regular cells, as shown in Fig. 2(a). There are more cells than that appeared in the critical state, for which the cell number should be about 10 [35], while Fig. 2(a) has illustrated 13 cells. This implies that the spatial wave length for this super-critical secondary flow is 1.538 ($=10\times2/13$). A pair of cells should have two different rotating behaviors, one rolling along the main stream direction, another cell takes the relevant reverse. One can see the cellular rolling behavior with respect to the isotherms shown in Fig. 2(b), which also indicates that the secondary flow has notable symmetry for the horizontal line $y = 0.5$ in this case.

However, this symmetrical property cannot appear for larger Rayleigh number cases. This can be seen from Fig. 3. It is noted that when the Rayleigh number is 20×10^4, the distribution of local Nusselt number on the bottom wall has lost its nearly regular periodic property.

Fig. 4 shows the evolution of the overall Nusselt number on the bottom wall for $S/W = 0.1$, $\theta = 45°$ when Ra varies from 10^4 to 100×10^4. At first, it can be seen that two regimes of natural convection appear. For larger Ra, the averaged Nusselt number has temporal oscillation. This means that the natural convection model may be invalid if the possible transition to chaos in the secondary flow is considered. Secondly, there is an initial variation period during which the Nusselt number decay gradually, and then it starts growing to a peak and varying to a steady state. The initial period is longer as the Rayleigh number is relatively small. The Nusselt number at the final state is smaller than the value measured, since the open ended effect has been totally

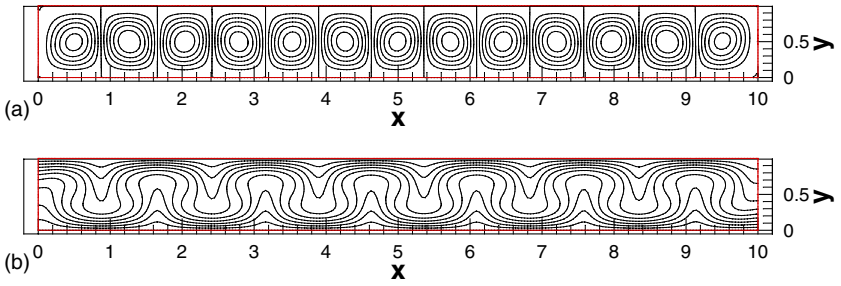

Fig. 2. (a) Streamlines for $Ra = 10^4$ at the moment $t = 200$. Note that these streamlines are labeled by values of $\psi^*(= \psi \times \sqrt{Ra/Pr}) = -1.0$, via 0–1.0 with an increment 0.2; (b) contours of temperature labeled by $\Theta = 0, 0.1, \ldots, 1$ with an increment 0.1.

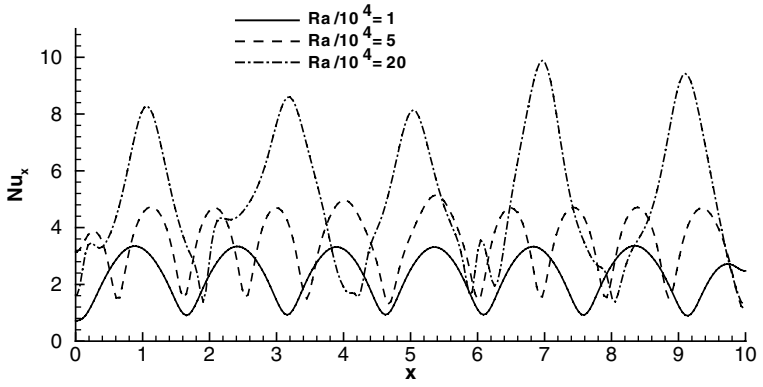

Fig. 3. Local Nusselt number on the bottom wall for different Rayleigh numbers.

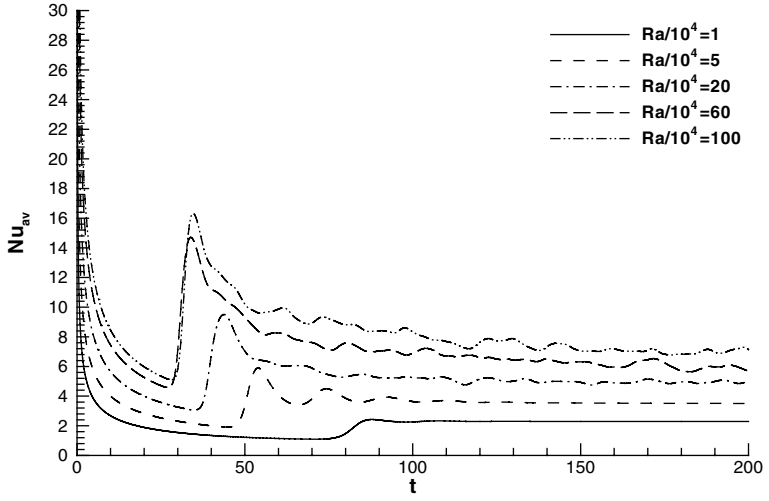

Fig. 4. Evolution of the overall Nusselt number on the bottom wall for various Rayleigh numbers.

ignored and the main stream is assumed as fully developed. However, as shown in Table 1, the Nusselt number has excellent agreement with the measured values for Benard thermal convection in a horizontal water layer [35,42]. The maximum deviation is less than 5%. It is seen that the Rayleigh number should be multiplied by a

Table 1
The overall Nusselt number on the bottom wall for the cases given in Fig. 4

$Ra\sin\theta/10^4$	0.707	3.536	14.14	42.43	70.71
Nu_{av} experiment [35,42]	2.28	3.03	4.65	6.53	7.53
Nu_{av} present calulation	2.20	3.05	4.80	6.20	7.25

factor $\sin\theta$. For the natural convection at the Ra range considered, the overall heat flux of the secondary flow for NCIC problem can be predicted by solving the Navier–Stokes equations.

4.3. Effect of the inclination

The numerical results have revealed that the secondary flow appears to have different patterns when the inclination of the channel varies from 15° to 45°. As shown in Fig. 5(a), for $Ra = 10^4$, when the inclination is 15°, the secondary flow is rather weak, because the stream function

$$\psi^*(=\psi\sqrt{Ra/Pr}, \partial\psi/\partial y = u, \partial\psi/\partial x = -v)$$

takes a small value, which is of the order 10^{-6}. However, for the case of larger inclination, Fig. 5(b) and (c) show that the value of ψ^* has an order of unity for the particular Rayleigh number. The inclination can also impact the number of cell in the secondary flow section. The evaluated cell number and its relation to the Ra and inclination have been given in Table 2.

To validate the cell number shown in Table 2, Figs. 6 and 7 show the secondary flow patterns for another spacing width ratio $S/W = 0.5$ with two Ra values ($Ra = 2.5\times10^4$, 1.495×10^5). It is noted that for small Rayleigh number, the inclination does not affect the uniformity of the cellular distribution in the flow section. However, for larger Ra value such as $Ra = 1.495\times10^5$, the inclination does cause the distribution uniformity of cells, but the cell number becomes less.

4.4. Effect of Rayleigh number

The Rayleigh number as an indication of heating rate should have a dominant effect on the secondary flow of NCIC as shown in Table 2. The extensive numerical experiments have confirmed the fact. However, the effect of Rayleigh number can be alleviated by decreasing the inclination of the channel for small Rayleigh numbers. When the Rayleigh number is beyond the threshold of the transition to chaos, which is about 10^5, the inclination effect nearly disappeared. Fig. 8 shows the streamlines corresponding to three Ra values as the ratio S/W is set as 0.0667, from which one also can see that the cell number given in Table 2 coincides with the evaluated pattern of the secondary flow of NCIC.

4.5. Effect of ratio S/W

The side walls effect is equivalent to the effect of the ratio S/W. Numerical results were evaluated by fixing the spacing and allowing the width to be changed. This, however, is different from the way used in laboratory, where the width is fixed and spacing of the channel can be adjusted to a required scale. It is convenient to assign

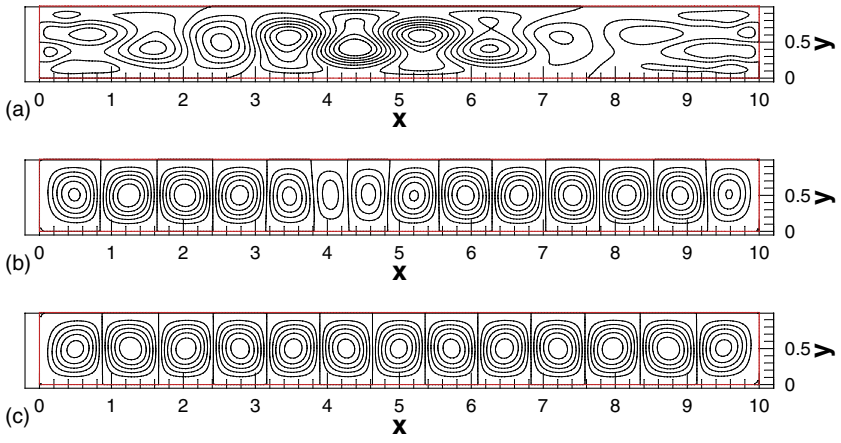

Fig. 5. The secondary flow patterns at $t = 200$ for $Ra = 10^4$ and $S/W = 0.1$ with (a) for $\theta = 15°$, (b) for $\theta = 30°$, and (c) for $\theta = 45°$. Note that these streamlines in (a), (b) and (c) are respectively labeled by values of $\psi^*(=\psi\times\sqrt{Ra/Pr}) = -1.0\times10^{-6}$, via 0 to $+1.0\times10^{-6}$ with an increment 2.0×10^{-6}; $\psi^* = -0.75$, via 0 to +0.75 with an increment 1.5; and $\psi^* = -1.0$, via 0 to +1.0 with an increment 0.2.

Table 2
The cell numbers in the super-critical secondary flow for different inclinations and Rayleigh numbers

$Ra/10^4$	$S/W = 0.1$			$S/W = 0.0667$			$S/W = 0.05$		
	$\theta = 15°$	$\theta = 30°$	$\theta = 45°$	$\theta = 15°$	$\theta = 30°$	$\theta = 45°$	$\theta = 15°$	$\theta = 30°$	$\theta = 45°$
1	10	14	13	15	20	18	19	24	23
2.5	13	13	15	20	23	22	26	27	29
5.0	15	18	19	20	22	21	28	30	33
14.95	17	14	12	24	18	15	44	29	24
20.0	17	11	10	20	16	16	38	29	19
40.0	11	12	10	15	16	14	26	20	19
60.0	11	9	10	19	15	14	24	18	19
80.0	13	10	10	16	14	14	20	17	18
100.0	12	9	10	15	16	14	20	17	19

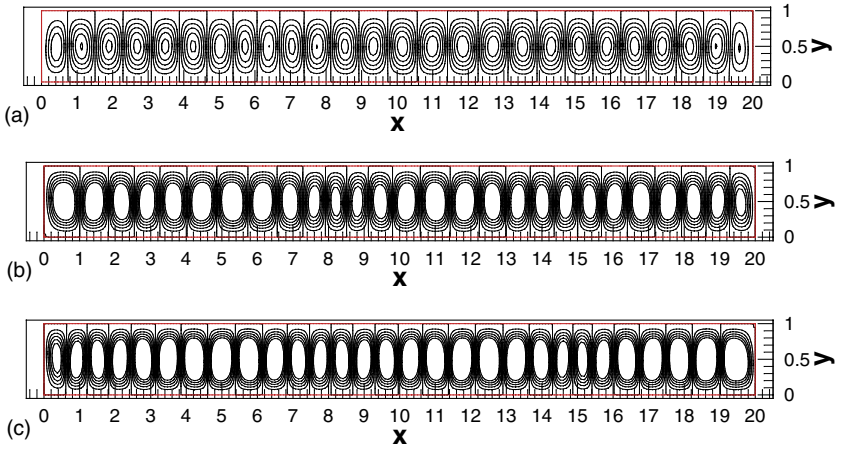

Fig. 6. The secondary flow patterns at $t = 200$ for $Ra = 2.5 \times 10^4$ and $S/W = 0.05$ with (a) for $\theta = 15°$, (b) for $\theta = 30°$, and (c) for $\theta = 45°$. Note that these streamlines in (a), (b), and (c) are labeled by values of $\psi^* = -1.0$, via 0 to +1.0 with an increment 0.2.

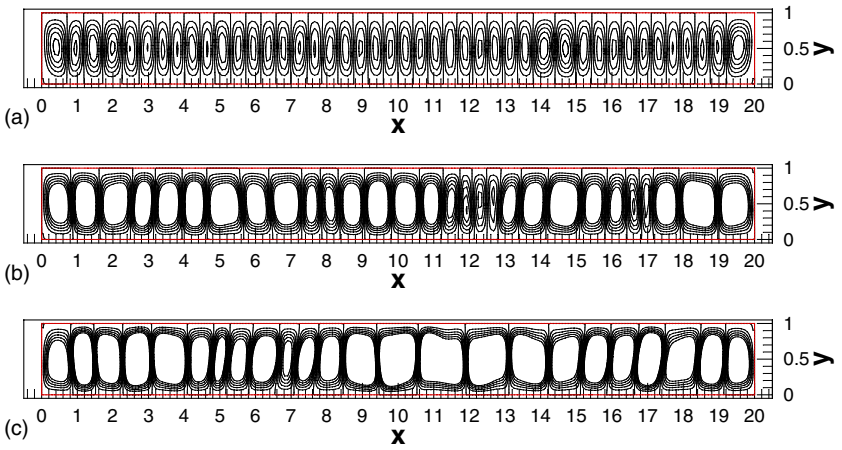

Fig. 7. The secondary flow patterns of NCIC at $t = 200$ for $Ra = 14.95 \times 10^4$ and $S/W = 0.05$ with (a) for $\theta = 15°$, (b) for $\theta = 30°$, and (c) for $\theta = 45°$. Note that these streamlines in parts (a), (b), and (c) are labeled by values of $\psi^* = -2.5$, via 0 to +2.5 with an increment 0.5.

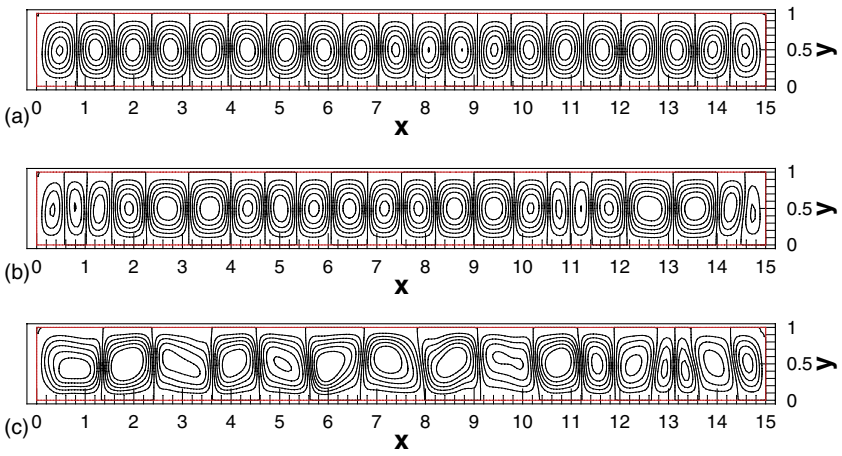

Fig. 8. The influence of Rayleigh number on the secondary flow patterns for (a) $Ra = 10^4$, (b) $Ra = 5 \times 10^4$, and (c) $Ra = 20 \times 10^4$. Note that these streamlines in (a), (b), and (c) are labeled respectively by values of $\psi^* = -1$, via 0 to +1 with an increment 0.2, −3 via 0 to +3.0 with an increment 0.6; and −7 via 0 to +7 with an increment 1.4.

the value of Rayleigh numbers in this way. Regardless of the scale choice and Ra values, the cell number becomes more when the ratio S/W is decreased. For instance, for $Ra = 10^4$, from the third row in Table 2, the cell number has changed from 14, via 20 to 24 for $\theta = 30°$, as the ratio S/W is varied from 0.1, via 0.667 to 0.05. From the remained rows in Table, this variation trend is the same.

4.6. Comparisons of spatial wavelength between simulation and test results

Fig. 9 shows the comparison of the numerical results with experimental data abstracted from Ref. [28], for the special inclination $\theta = 45°$. In Ref. [28], Azevedo and Sparrow have shown their correlation for the spatial wavelength as $L_x/S = 26.2Ra^{-0.3}$. In general, the predicted wave length is larger than the measured data. The predicted results are in good agreement with the experimental results for smaller Rayleigh numbers ($Ra < 10^5$). For Rayleigh number over the second threshold of flow instability, i.e. the transition to chaos, larger discrepancies are found. The deviation may be caused by the channel's open end influence, which was not considered in the numerical simulations. The results shown in Table 1 have revealed that the overall Nusselt numbers from calculation agree with the early measurements [35,42] quite well. It seems difficult to say that the calculation may be unrealitic for those cases with larger Ra (>10^5).

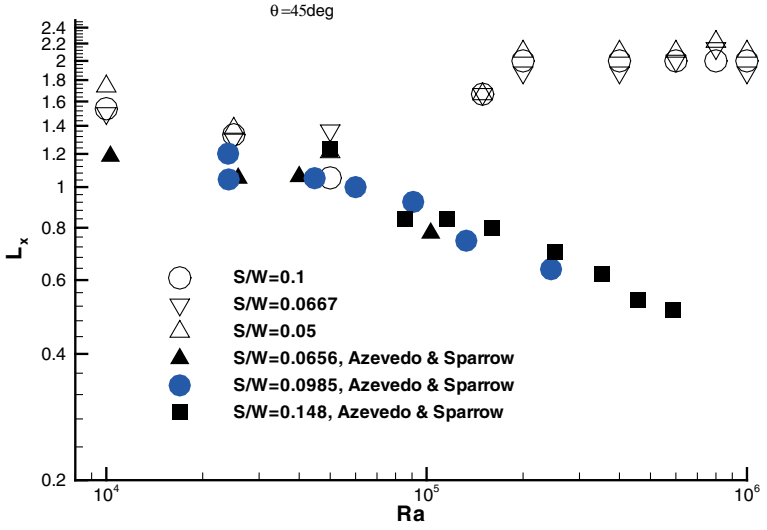

Fig. 9. Comparison of the spatial wavelength between numerical simulation and experimental results for the case $\theta = 45$ °C.

In addition, the numerical viscous effect becomes apparant for the case of large Rayleigh numbers. The deviation means that the feasibility of using finite difference approximation in these cases is doubtful. Even though the ratio of spacing to width has impacted the cellular number, the wave length of the cells for the secondary flow, as shown in Fig. 9, is almost independent of the ratio.

5. Conclusions

The super-critical properties of secondary flow of natural convection in inclined channels (NCIC) have been explored numerically with PmIII algorithm, in which, the inclination and the side wall effects have been emphasized. The results show that the secondary flow patterns is dominated by Rayleigh number when the Prandtl number is fixed for water flow, but the inclination of the inclined channel has significant influence on the cellular number appeared in the secondary flow.

Decreasing the ratio of spacing to width increases the cell number. However, as indicated in the experimental results, the spatial wave length in the secondary flow is almost independent of the ratio. For relatively small Rayleigh number, the predicted results are well compared with the measured data, implying the numerical method is applicable to capture the properties of the secondary flows of NCIC for moderate Rayleigh numbers. However, for larger Rayleigh numbers, the secondary flow for NCIC appears to have less cells than observed. This may be caused by neglecting the channel's open end effect. It should be noted that for this case, the feasibility of the finite difference approximation is questionable due to the presence of apparent viscous effect.

Acknowledgements

This work is financially supported by the Research Grants Council of the Hong Kong SAR Government with Project No.: PolyU 5033/00E.

References

[1] W. Elenbaas, Heat dissipation of parallel plates by free convection, Physica 9 (1942) 1–28.
[2] J.R. Bodoia, J.F. Osterle, The development of free convection between heated vertical plates, J. Heat Transfer 84 (1962) 40–44.
[3] W. Aung, L.S. Fletcher, V. Sernas, Developing laminar free convection between vertical flat plates with asymmetric heating, Int. J. Heat Mass Transfer 15 (1972) 2293–2308.
[4] W. Aung, G. Worku, Developing flow and flow reversal in a vertical channel with assymmetric wall temperatures, J. Heat Transfer 108 (2) (1986) 299–304.
[5] W. Aung, G. Worku, Theory of fully developed, combined convection including flow reversal, J. Heat Transfer 108 (2) (1986) 485–488.
[6] E.M. Sparrow, G.M. Chrysler, L.F. Azevedo, Observed flow reversal and measured-predicted Nusselt numbers for natural convection in a one-sided heated vertical channel, J. Heat Transfer 106 (1984) 325–332.
[7] R.A. Wirtz, L.H. Liu, Numerical experiments on the onset of layered convection in a narrow slot containing a stably stratified fluid, Int. J. Heat Mass Transfer 18 (1975) 1299–1305.
[8] E. Zanchini, Effect of viscous dissipation on mixed convection in a vertical channel with boundary conditions of third kind, Int. J. Heat Mass Transfer 41 (1998) 3949–3959.
[9] A. Barletta, Laminar mixed convection with viscous dissipation in a vertical channel, Int. J. Heat Mass Transfer 41 (1998) 3501–3513.
[10] A. Barletta, Analysis of combined forced and free flow in a vertical channel with viscous dissipation and isothermal-isoflux boundary conditions, J. Heat Transfer 121 (2) (1999) 349–356.
[11] A. Barletta, E. Zanchini, Time period laminar mixed convection in an inclined channel, Int. J. Heat Mass Transfer 46 (3) (2003) 551–563.
[12] V.A.F. Costa, Laminar natural convection in differentially heated rectangular enclosure with vertical diffusive walls, Int. J. Heat Mass Transfer 45 (20) (2002) 4217–4225.
[13] Q.H. Deng, G.F. Tang, Y.G. Li, M.Y. Ha, Interaction between discrete heat source in horizontal natural convection enclosures, Int. J. Heat Mass Transfer 45 (26) (2002) 5117–5132.
[14] K. Khanafer, K. Vafai, M. Lightstone, Mixed convection heat transfer in two dimensional open-ended enclosures, Int. J. Heat Mass Transfer 45 (26) (2002) 5171–5190.
[15] L. Adjlout, O. Imine, A. Azzi, M. Belkadi, Laminar natural convection in an inclined cavity with a wavy wall, Int. J. Heat Mass Transfer 45 (10) (2002) 2141–2152.
[16] K.T. Lee, W.M. Yan, Mixed convection heat transfer in horizontal rectangular ducts with wall transpiration effects, Int. J. Heat Mass Transfer 41 (2) (1998) 411–423.
[17] Y.L. Chan, C.L. Tien, Laminar natural convection in shallow open cavities, J. Heat Transfer 108 (1986) 305–309.
[18] K. Vafai, C.P. Desai, S.V. Lyer, M.P. Dyko, Buoyancy induced convection in a narrow open-ended annulus, J. Heat Transfer 119 (3) (1997) 483–494.
[19] C.L. Chen, C.H. Cheng, Buoyancy-induced flow and convective heat transfer in an inclined arc-shape enclosure, Int. J. Heat Fluid Flow 23 (6) (2002) 823–830.
[20] Y.C. Chen, J.N. Chung, The linear stability of mixed convection in a vertical channel flow, J. Fluid Mech. 325 (1996) 29–51.
[21] Y.C. Chen, J.N. Chung, Stability of mixed convection in a differentially heated vertical channel, J. Heat Transfer 120 (1) (1998) 127–133.
[22] P. Le Quéré, Transition to unsteady natural convection in a tall water-filled cavity, Phys. Fluid A 2 (4) (1990) 503–515.
[23] P. Le Quéré, M. Behnia, From onset of unsteadiness to chaos in a differentially heated square cavity, J. Fluid Mech. 359 (1998) 81–107.

[24] S. Wakitani, Numerical study of three dimensional oscillatory natural convection at low Prandtl number in rectangular enclosures, J. Heat Transfer 123 (2001) 77–83.
[25] H. Luz Neto, J.N.N. Quaresma, R.M. Cotta, Natural convection in three-dimensional porous cavities: integral transform method, Int. J. Heat Mass Transfer 45 (14) (2002) 3013–3032.
[26] J. Pallares, I. Cuesta, F.X. Grau, Laminar and turbulent Rayleigh–Bénard convection in a perfectly conducting cubical cavity, Int. J. Heat Fluid Flow 23 (3) (2002) 346–358.
[27] S.K.W. Tou, X.F. Zhang, Three-dimensional numerical simulation of natural convection in an inclined liquid-filled enclosure with an array of discrete heaters, Int. J. Heat Mass Transfer 46 (1) (2003) 127–138.
[28] L.F.A. Azevedo, E.M. Sparrow, Natural convection in open-ended inclined channels, J. Heat Transfer 107 (1985) 893–901.
[29] A.S. Lavine, On the linear stability of mixed and free convection between inclined parallel plates with fixed heat flux boundary conditions, Int. J. Heat Mass Transfer 36 (5) (1993) 1373–1387.
[30] H.X. Yang, Z.J. Zhu, J. Gilleard, Numerical simulation of thermal fluid instability between two horizontal parallel plates, Int. J. Heat Mass Transfer 44 (2001) 1485–1493.
[31] D.L. Brown, R. Cortez, M.L. Minion, Accurate projection methods for the incompressible Navier–Stokes equations, J. Comput. Phys. 168 (2001) 464–499.
[32] T.J. Baker, Potential flow calculation by the approximate factorization method, J. Comput. Phys. 42 (1981) 1–19.
[33] Z.J. Zhu, H.X. Yang, Numerical investigation of transient laminar natural convection of air in a tall cavity, Heat Mass Transfer 39 (2003) 579–587.
[34] H.X. Yang, Z.J. Zhu, Numerical study on transient laminar natural convection in an inclined parallel-walled channel, Int. Commun. Heat Mass Transfer 30 (2003) 359–367.
[35] S. Chandrasekhar, Hydrodynamic and Hydromagnetic Stability, Oxford, 1961, pp. 1–74.
[36] P. Le Quéré, T.A.D. Roquefort, Computation of natural convection in two-dimensional cavities with Chebyshev polynomials, J. Comput. Phys. 57 (1985) 210–228.
[37] S.H. Xin, P. Le Quéré, L.S. Tuckerman, Bifurcation analysis of double-diffusive convection with opposing horizontal thermal solutal gradient, Phys. Fluids A 10 (4) (1998) 850–858.
[38] S. Wakitani, Development of multicellular solution in natural convection in an air-filled vertical cavity, J. Heat Transfer 119 (1996) 97–101.
[39] T. Kawamura, K. Kawahara, Computation of high Reynolds number flow around a circular cylinder with surface roughness, AIAA paper (1984) No. 84-0340.
[40] S.V. Patankar, Numerical Heat Transfer and Fluid Flow, Hemisphere, 1980.
[41] E. Papanicolaou, Y. Jaluria, Transition to a periodic regime in mixed convection in a square cavity, J. Fluid Mech. 239 (1992) 489–509.
[42] P.L. Silvestuon, Wärmedurchgang in Waagerechten Flüssigkeitsschichten, Part 1, Forsch. Ing. Wes. 24 (1958) 29–32, 59–69.